Transport Properties of Spin Field-Effect Transistors Built on Si and InAs

D. Osintsev, V. Sverdlov, Z. Stanojević, A. Makarov, and S. Selberherr

Institute for Microelectronics, Technische Universität Wien
Gußhausstraße 27-29, A-1040 Wien, Austria
E-mail: {osintsev|sverdlov|stanojevic|makarov|selberherr}@iue.tuwien.ac

1. Abstract

We investigate the properties of ballistic spin field-effect transistors (SpinFETs). First we show that the amplitude of the tunneling magnetoresistance oscillations decreases dramatically with increasing temperature in SpinFETs with the semiconductor channel made of InAs. We also demonstrate that the [100] orientation of the silicon fin is preferred for practical realizations of silicon SpinFETs due to stronger modulation of the conductance as a function of spin-orbit interaction and magnetic field.

2. Introduction

Utilizing spin properties of electrons for future microelectronic devices opens great opportunities to reduce device power consumption. In recent years spintronic devices have received much attention, where the spin of the electron is used as additional degree of freedom to tune the properties of a transistor. The spin field-effect transistor (SpinFET) is a future semiconductor spintronic device promising to achieve a performance superior to that achieved in the present transistor technology. SpinFETs are composed of two ferromagnetic contacts (source and drain), which sandwich the semiconductor region. Ferromagnetic contacts contain mostly spin-polarized electrons and play the role of polarizer and analyzer as described by Datta and Das [1]. The ferromagnetic source contact injects spin-polarized electrons to the semiconductor region. Because of the non-zero spin-orbit interaction the electron spin precesses during the propagation through the channel. At the drain contact only the electrons with spin aligned to the drain magnetization can leave the channel and contribute to the current. Current modulation is achieved by changing the strength of the spin-orbit interaction in the semiconductor region and thus the degree of the spin precession. Spin-orbit interaction can be controlled by an applying external gate voltage which introduces structural inversion asymmetry.

The dominant mechanism of the spin-orbit coupling is usually taken in the Rashba form [2]. The corresponding effective Hamiltonian is

$$H_R = \frac{\alpha_R}{\hbar}(p_x\sigma_y - p_y\sigma_x), \quad (1)$$

where α_R is the effective electric field-dependent parameter of the spin-orbit interaction, $p_{x(y)}$ is the electron momentum projection, σ_x and σ_y are the Pauli matrices.

Silicon has a weak spin-orbit interaction and long spin life time. It is therefore an attractive material for spin current propagation. However, because of its weak spin-orbit interaction, silicon was not considered as a candidate for the SpinFET channel material. Recently, however, it was shown [3] that thin silicon films inside SiGe/Si/SiGe structures have large values of spin-orbit interaction. Interestingly, the strength of the Rashba spin-orbit interaction is relatively small and is approximately ten times smaller than the value of the dominant contribution which is of the Dresselhaus type with a corresponding effective Hamiltonian in the form

$$H_R = \frac{\beta}{\hbar}(p_x\sigma_x - p_y\sigma_y), \quad (2)$$

This major contribution to the spin-orbit interaction is due to interfacial disorder induced inversion symmetry breaking and depends almost linearly on the effective electric field [4]. For a built-in field 50kV/cm, the strength of the Dresselhaus spin-orbit interaction is found to be $\beta \approx 2$μeVnm, which is in agreement with the value found experimentally [5], while $\alpha_R \approx 0.1$μeVnm. This value of the spin-orbit interaction in confined silicon systems is sufficient for their applications as SpinFET channels.

The stronger spin-orbit interaction leads to an increased spin relaxation. The D'yakonov-Perel' mechanism is the main spin relaxation mechanism in systems, where the electron dispersion curves for the two spin projections are non-degenerate. In quasi-one-dimensional electron structures, however, a suppression of the this spin relaxation mechanism is expected [6]. Indeed, in case of elastic scattering only back-scattering is allowed. Reversal of the electron momentum results in the inversion of the effective magnetic field direction. Therefore, the precession angle does not depend on the number of scattering events along the carrier trajectory in the channel, but is a function of the channel length only. Thus, the spin-independent elastic scattering does

978-1-4577-0091-0/11/$26.00 ©2011 IEEE

not result in additional spin decoherence. In the presence of an external magnetic field, however, spin-flip processes become possible, and the Elliott-Yafet spin relaxation mechanism is likely activated [7].

3. Model

To calculate the properties of the ballistic spin field-effect transistor we consider a model similar to [7] and [8]. The Hamiltonian in the ferromagnetic regions has the following form in the one-band effective mass approximation

$$\hat{H}_F^L = \frac{\hat{p}_x^2}{2m_f^*} + h_0\hat{\sigma}_z, \quad x < 0, \tag{3}$$

$$\hat{H}_F^R = \frac{\hat{p}_x^2}{2m_f^*} \pm h_0\hat{\sigma}_z, \quad x > L, \tag{4}$$

where m^*_f is the effective mass in the contacts, $h_0=2PE_F/(P^2+1)$ is the exchange splitting energy with P defined as the spin polarization in the ferromagnetic regions, E_F is the Fermi energy, and σ_z is the Pauli matrix; ± in (4) stands for the parallel and anti-parallel configurations of the contact magnetization. For the silicon channel region the Hamiltonian reads [7], [8]

$$\hat{H}_S = \frac{\hat{p}_x^2}{2m_s^*} + \delta E_c - \frac{\alpha_R}{\hbar}\hat{\sigma}_y\hat{p}_x + \frac{1}{2}g\mu_B B\hat{\sigma}^*,$$

where m^*_s is the subband effective mass, δE_c is the band mismatch between the ferromagnetic and the semiconductor region, α_R is the strength of the spin-orbit interaction, g is the Landé factor, μ_B is the Bohr magneton, B is the magnetic field, and $\hat{\sigma}^* \equiv \hat{\sigma}_x\cos\gamma + \hat{\sigma}_y\sin\gamma$ with γ defined as the angle between the magnetic field and the transport direction.

To calculate the dependence of the transport properties on the spin-orbit interaction we need the electron eigenfunctions in the various regions. For the ferromagnetic regions spin-up and spin-down eigenstates have the form $(1, 0)^\dagger$ and $(0, 1)^\dagger$, respectively. The wave function in the left contact has the following form:

$$\Psi_L(x) = (e^{ik_\uparrow x} + R_\uparrow e^{-ik_\uparrow x})\begin{pmatrix}1\\0\end{pmatrix} + R_\downarrow e^{-ik_\downarrow x}\begin{pmatrix}0\\1\end{pmatrix}, \tag{5}$$

$$\Psi_L(x) = R_\uparrow e^{-ik_\uparrow x}\begin{pmatrix}1\\0\end{pmatrix} + (e^{ik_\downarrow x} + R_\downarrow e^{-ik_\downarrow x})\begin{pmatrix}0\\1\end{pmatrix}, \tag{6}$$

where (5) represents the incoming spin-up electrons and (6) the incoming spin-down electrons, correspondingly, $k_{\uparrow(\downarrow)} = \sqrt{2m_f^*(E \mp h_0)/\hbar^2}$ is the wave vector of the spin-up (spin-down) electron and $R_{\uparrow(\downarrow)}$ is the amplitude of the reflected wave. For the right contact the wave function is given by

$$\Psi_R(x) = C_\uparrow e^{ik_\uparrow x}\begin{pmatrix}1\\0\end{pmatrix} + C_\downarrow e^{ik_\downarrow x}\begin{pmatrix}0\\1\end{pmatrix}.$$

For the semiconductor region the wave function can be written as

$$\Psi_S(x) = A_+ e^{ik_{x1}^{(+)}x}\begin{pmatrix}k_1\\1\end{pmatrix} + B_+ e^{ik_{x2}^{(+)}x}\begin{pmatrix}k_2\\1\end{pmatrix}$$
$$A_- e^{ik_{x1}^{(-)}x}\begin{pmatrix}k_3\\-1\end{pmatrix} + B_- e^{ik_{x2}^{(-)}x}\begin{pmatrix}k_4\\-1\end{pmatrix},$$

where $k_{x1(x2)}^{(+)}$ and $k_{x1(x2)}^{(-)}$ are the wave vectors obtained by solving the equations $\frac{\hbar^2k^2}{2m_s^*} + \delta E_c \pm \sqrt{\left(\frac{Bg\mu_B\cos(\gamma)}{2}\right)^2 + \left(\frac{Bg\mu_B\sin(\gamma)}{2} - \alpha_R k\right)^2} = E$, respectively.

The constants k_1, k_2, k_3, k_4 are calculated as

$$k_1 = -\frac{i\left(Bg\mu_B\sin(\gamma) - 2\alpha_R k_{x1}^{(+)}\right) - Bg\mu_B\cos(\gamma)}{2\sqrt{\left(\frac{Bg\mu_B\cos(\gamma)}{2}\right)^2 + \left(\frac{Bg\mu_B\sin(\gamma)}{2} - \alpha_R k_{x1}^{(+)}\right)^2}},$$

$$k_2 = -\frac{i\left(Bg\mu_B\sin(\gamma) - 2\alpha_R k_{x2}^{(+)}\right) - Bg\mu_B\cos(\gamma)}{2\sqrt{\left(\frac{Bg\mu_B\cos(\gamma)}{2}\right)^2 + \left(\frac{Bg\mu_B\sin(\gamma)}{2} - \alpha_R k_{x2}^{(+)}\right)^2}},$$

$$k_3 = \frac{i\left(Bg\mu_B\sin(\gamma) - 2\alpha_R k_{x1}^{(-)}\right) - Bg\mu_B\cos(\gamma)}{2\sqrt{\left(\frac{Bg\mu_B\cos(\gamma)}{2}\right)^2 + \left(\frac{Bg\mu_B\sin(\gamma)}{2} - \alpha_R k_{x1}^{(-)}\right)^2}},$$

$$k_4 = \frac{i\left(Bg\mu_B\sin(\gamma) - 2\alpha_R k_{x2}^{(-)}\right) - Bg\mu_B\cos(\gamma)}{2\sqrt{\left(\frac{Bg\mu_B\cos(\gamma)}{2}\right)^2 + \left(\frac{Bg\mu_B\sin(\gamma)}{2} - \alpha_R k_{x2}^{(-)}\right)^2}}.$$

The reflection and transmission coefficients are determined by applying the boundary conditions at the ferromagnet/semiconductor interfaces.

We compute the current through the device as

$$I^{P(AP)}(V) = \frac{e}{h}\int_{\delta E_c}^{\infty}\left[T_\uparrow^{P(AP)}(E) + T_\downarrow^{P(AP)}(E)\right]$$
$$\left\{\frac{1}{1+e^{\frac{E-E_F}{k_BT}}} - \frac{1}{1+e^{\frac{E-E_F+eV}{k_BT}}}\right\}dE,$$

where k_B is the Boltzmann constant, T is the temperature, V is the voltage. The spin-up ($T^P_\uparrow$) and spin-down ($T^P_\downarrow$) transmission probability for the parallel configuration of the contact magnetization is defined as

$$T_\uparrow^P = \left|C_\uparrow\right|^2 + \frac{k_\downarrow}{k_\uparrow}\left|C_\downarrow\right|^2,$$

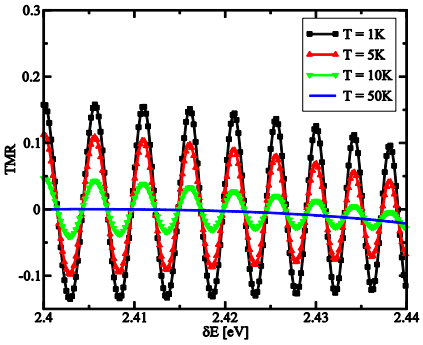

Fig.1: *TMR dependence on the value of δE, for EF =2.47eV, eV =0.001eV, R =31.7meVnm without magnetic field.*

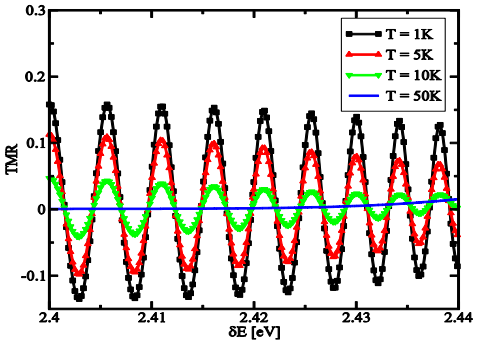

Fig.2: *Same as in Fig. 1 with a magnetic field of 3T.*

$$T_{\downarrow}^{P} = \frac{k_{\uparrow}}{k_{\downarrow}}\left|C_{\uparrow}\right|^2 + \left|C_{\downarrow}\right|^2.$$

For the anti-parallel configuration of contact magnetization transmission probability is given by

$$T_{\uparrow}^{AP} = \frac{k_{\downarrow}}{k_{\uparrow}}\left|C_{\uparrow}\right|^2 + \left|C_{\downarrow}\right|^2,$$

$$T_{\downarrow}^{AP} = \left|C_{\uparrow}\right|^2 + \frac{k_{\uparrow}}{k_{\downarrow}}\left|C_{\downarrow}\right|^2.$$

The conductance is defined as

$$G^{P(AP)} = \lim_{V\to 0}\frac{I^{P(AP)}}{V}.$$

In the limit of low temperature the conductance must coincide with the one obtained from the Laudauer-Büttiker formula

$$G^{P(AP)} = \frac{e^2}{h}\left(T_{\uparrow}^{P(AP)}(E_F) + T_{\downarrow}^{P(AP)}(E_F)\right).$$

Finally, the tunneling magnetoresistance (TMR) is defined as

$$TMR \equiv \frac{G_P - G_{AP}}{G_{AP}}.$$

3. Results and Discussion

We present the results of our simulations for SpinFETs using InAs and Si as the channel material.

A. InAs Calculations

For the calculations of InAs channel devices we assume effective masses for the ferromagnetic region $m^*_f = m_0$ and for the semiconductor region $m^*_s = 0.036m_0$, where m_0 is the electron rest mass. The length of the channel is set to 0.3μm.

Fig. 1 and Fig. 2 show the dependence of the TMR on the band mismatch between the source/drain contacts and the semiconductor region, for several temperatures in absence of magnetic field and under an applied field of 3T. At low temperatures the TMR oscillates around zero, and the strength of the magnetic field does not influence the oscillations much, which is in the agreement with [8]. As the band mismatch increases, influence of the magnetic field becomes more significant. Also, one can see that increasing the temperature leads to a dramatic decrease in the amplitude of the TMR oscillations and reduces the ability to modulate the TMR by adjusting the band mismatch.

B. Si Calculations

We consider square silicon fins of [100] and [110] orientations, with (001) horizontal faces. The parabolic band approximation is not sufficient in thin and narrow silicon fins. In order to compute the subband structure in silicon fins we employ the two-band **k·p** model proposed in [9], which has been shown to be accurate up to 0.5eV above the conduction band edge [10]. The resulting Schrödinger differential equation, with the confinement potential appropriately added in the Hamiltonian [9], is discretized using the box integration method and solved for each value of the conserved momentum p_x along the current direction using efficient numerical algorithms available through the Vienna Schrödinger-Poisson framework (VSP) [11].

Fig. 3 demonstrates the dependence of the subband minima as function of the fin thickness *t* for the lowest four subbands; the fin orientation is along the [110] direction. The dependence of the splitting between the unprimed subbands with decreasing *t*, which are perfectly degenerate in the effective mass approximation, is clearly seen. Splitting between valleys in a [100] fin can be ignored [12]. In contrast to that, the dependence of the effective mass of the ground subband in [100] fins on *t* is more pronounced as compared to [110] fins. Results of density-functional calculations [12] confirm the mass dependences obtained from the **k·p** model (Fig. 4). With the values of the effective masses and subband offsets obtained, we study the conductance properties for the parallel and anti-parallel configurations of the contact magnetization. The spin-

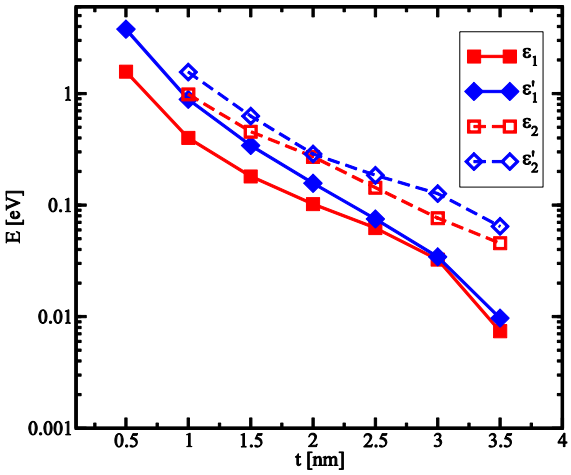

Fig.3: *Subband minima as a function of thickness t in a [110] fin.*

orbit interaction is treated in the Dresselhaus form (2). The Hamiltonian in the channel reads

$$\hat{H}_S = \sum_n \frac{\hat{p}_x^2}{2m_n^*} + \delta E_n - \frac{\beta}{\hbar}\hat{\sigma}_x \hat{p}_x + \frac{1}{2} g\mu_B B\hat{\sigma}^*,$$

for [100] oriented fins and

$$\hat{H}_S = \sum_n \frac{\hat{p}_x^2}{2m_n^*} + \delta E_n - \frac{\beta}{\hbar}\hat{\sigma}_y \hat{p}_x + \frac{1}{2} g\mu_B B\hat{\sigma}^*,$$

for [110] oriented fins. Here m^*_n is the subband effective mass, δE_n is the subband mismatch between the ferromagnetic region and the channel, and β is the strength of the spin-orbit interaction.

Fig. 5 shows the dependence of the TMR for [100] and [110] oriented fins with t = 1.5nm on the value of the spin-orbit interaction. Fins of [100] orientation shows a stronger dependence on β compared to [110] oriented fins. Thus [100] oriented fins are preferred for silicon SpinFETs. The reason of the stronger dependence is that the strength of the spin-orbit interaction is defined by the wave vector $k_D = m^*_n\beta/\hbar^2$. As it is shown in Fig. 4, the effective mass value for the

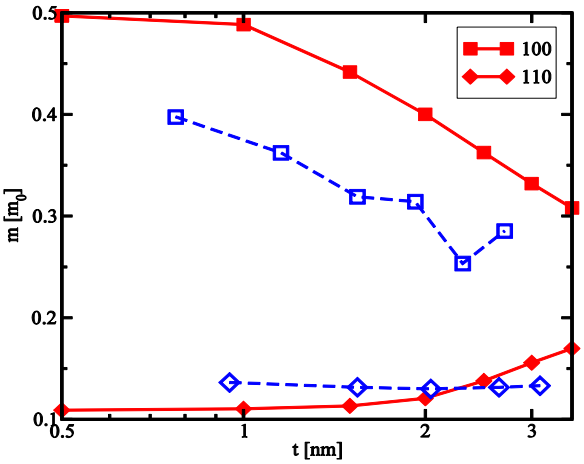

Fig.4: *Ground subband effective mass dependence on t in [100] and [110] fins. Open symbols are from [12].*

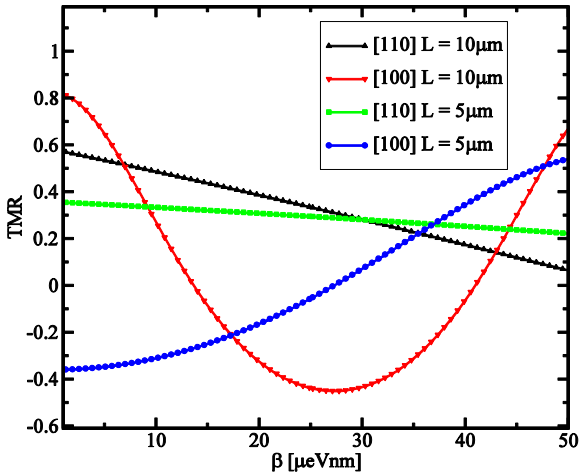

Fig.5: *TMR dependence on the value of the Dresselhaus spin-orbit interaction for t = 1.5nm, B = 4T, P = 0.6, z = 3, γ = 0.*

[110] oriented fins is smaller compared to the [100] oriented fins, hence for the same variation of k_D in case of the [110] oriented fins a lager variation of β is required to achieve the same TMR value.

4. Summary and Conclusion

A possibility to build SpinFETs by using silicon fins has been investigated. The spin-orbit interaction due to the interface-induced inversion symmetry breaking is treated in the Dresselhaus form. It was shown that [100] fins are best suitable for practical realizations of silicon SpinFETs.

4. Summary and Conclusion

This work is supported by the European Research Council through the grant #247056 MOSILSPIN.

References

[1] S. Datta and B. Das, Applied Physics Letters **56**, 665 (1990).
[2] S. Giglberger *et al.*, Phys. Rev. B **75**, 035327 (2007).
[3] M. O. Nestoklon, E. L. Ivchenko, J.-M. Jancu, and P. Voisin, Phys. Rev. B **77**, 155328 (2008).
[4] M. Prada, G.Klimeck, and R. Joynt, cond-mat 0908.2417 (2009).
[5] Z. Wilamowski and W. Jantsch, Phys. Rev. B **69**, 035328 (2004).
[6] A. Bournel, P. Dollfus, B. P., and P. Hesto, European Phys. J. Appl. Phys. **4**, 1 (1998).
[7] M. Cahay and S. Bandyopadhyay, Phys. Rev. B **69**, 045303 (2004).
[8] K. Jiang *et al.*, IEEE T-ED 2005 (2010).
[9] G. L. Bir and G. E. Pikus, *Symmetry and strain-induced effects in semiconductors* (Wiley, 1974), p. 484.
[10] V. Sverdlov, O. Baumgartner, T. Windbacher, and S. Selberherr, J.Comput.Electronics **8**, 192 (2009).
[11] M. Karner *et al.*, J.Comput.Electronics **6**, 179 (2007).
[12] H. Tsuchiya *et al.*, IEEE Transactions on Electron Devices **57**, 406 (2010).